

Alma Mater Studiorum Università di Bologna  
Archivio istituzionale della ricerca

Features and application of coupled cold plasma and photocatalysis processes for decontamination of water

This is the final peer-reviewed author's accepted manuscript (postprint) of the following publication:

*Published Version:*

Berardinelli A., Hamrouni A., Dire S., Ceccato R., Camera-Roda G., Ragni L., et al. (2021). Features and application of coupled cold plasma and photocatalysis processes for decontamination of water. CHEMOSPHERE, 262(January 2021), 1-11 [10.1016/j.chemosphere.2020.128336].

*Availability:*

This version is available at: <https://hdl.handle.net/11585/784024> since: 2021-01-20

*Published:*

DOI: <http://doi.org/10.1016/j.chemosphere.2020.128336>

*Terms of use:*

Some rights reserved. The terms and conditions for the reuse of this version of the manuscript are specified in the publishing policy. For all terms of use and more information see the publisher's website.

This item was downloaded from IRIS Università di Bologna (<https://cris.unibo.it/>).  
When citing, please refer to the published version.

(Article begins on next page)

# Features and application of coupled cold plasma and photocatalysis processes for decontamination of water

Annachiara Berardinelli<sup>a,b</sup>, Abdessalem Hamrouni<sup>c</sup>, Sandra Dirè<sup>a</sup>, Riccardo Ceccato<sup>a</sup>, Giovanni Camera-Roda<sup>d</sup>, Luigi Ragni<sup>e,f</sup>, Leonardo Palmisano<sup>g</sup>, Francesco Parrino<sup>a\*</sup>

<sup>a</sup> Department of Industrial Engineering, University of Trento, Via Sommarive 9, 38123 Trento, Italy;

<sup>b</sup> Centro Agricoltura Alimenti Ambiente – C3A, University of Trento, Via E. Mach 1, 38010 S. Michele all'Adige (TN), Italy;

<sup>c</sup> Laboratoire de Recherche Catalyse et Matériaux pour l'Environnement et les Procédés URCMEP (UR11ES85), Faculté des Sciences de Gabès/Université de Gabès, Campus Universitaire Cité Erriadh, Gabès 6072, Tunisia;

<sup>d</sup> Department of Civil, Chemical, Environmental, and Materials Engineering, University of Bologna, via Terracini 28, Bologna (40131), Italy;

<sup>e</sup> Dipartimento di Scienze e Tecnologie Agro-Alimentari, University of Bologna, Piazza Goidanich 60, 47521 Cesena (FC), Italy;

<sup>f</sup> Interdepartmental Centre for Agri-Food Industrial Research, Alma Mater Studiorum, University of Bologna, Via Quinto Bucci, 336, 47521 Cesena (FC), Italy;

<sup>g</sup> Dipartimento di Ingegneria, University of Palermo, Viale delle Scienze Ed. 6, Palermo (90128), Italy.

\*Correspondence: mail: [francesco.parrino@unitn.it](mailto:francesco.parrino@unitn.it); tel: +39 0461 285295

## Abstract

Dielectric barrier discharge plasma and photocatalysis have been proposed as tools for decontamination of process water, especially in food industry. The present investigation aims to redefine and identify the features of coupling the two technologies in terms of degradation efficiency of a model compound. Results show that, when the process is carried out in plasma activated water in the presence of irradiated TiO<sub>2</sub>, the efficiency of the integrated process is lower than the sum of the two processes acting separately. It is proposed that afterglow species, e.g. hydrogen peroxide and/or peroxyxynitrites could be activated by UVA light irradiation producing hydroxyl radicals in the liquid phase. Even if TiO<sub>2</sub> limits this additional effect by acting as UVA screen barrier material, its decontamination efficiency under certain conditions results higher than that obtained with plasma systems. These results open the route to chlorine-free decontamination processes and redefine the application framework of this integrated approach.

35 **Keywords:** TiO<sub>2</sub> photocatalysis, Dielectric barrier discharge plasma, UVA light, process  
36 intensification, water decontamination.

37

## 38 **1. Introduction**

39 The decontamination of fresh cut fruits and vegetables poses several safety issues and is challenging  
40 due to the huge amount of drinking water needed (ca. 40 m<sup>3</sup> per ton of product). In fact, these products  
41 are generally eaten uncooked, and contamination could occur during different production steps  
42 (Meireles et al., 2016). Chlorine is widely applied to this aim, but it does not generally afford  
43 mineralization of residual antibiotics and/or pesticides eventually present and, worse still, produces  
44 carcinogenic and mutagenic chlorinated compounds which then accumulate in the process water.

45 Different alternative approaches, mainly based on advanced oxidation processes, were deeply  
46 investigated (Barbosa-Cánovas et al., 2017, Bhilwadikar et al., 2019). Among them, as witnessed by  
47 the increasing number of published researches, the use of cold plasma under atmospheric conditions  
48 could combine decontamination efficiency, process safety, and the need to preserve the organoleptic  
49 features of the products (Berardinelli et al., 2016). In fact, glowing plasma discharge above the  
50 aqueous phase to be decontaminated (plasma activated water, PAW) (Shen et al., 2016) has been  
51 proposed as a viable alternative to chlorine based sanitizers. Various devices working in different  
52 conditions (direct current, low frequency, radio frequency and microwave discharges), with peculiar  
53 geometries, energy demand, and in the presence of various gas mixtures can be used to drive the  
54 discharge. Among the low frequency plasma sources, Dielectric Barrier Discharge (DBD) devices  
55 are, undoubtedly, the most investigated and industrialized non-equilibrium plasma generators. In a  
56 DBD device the discharge is driven by applying alternating current between two electrodes often  
57 characterized by a separation gap of few millimetres and by one or more dielectric layers. DBD  
58 presents relevant advantages in terms of costs, flexibility, operating parameters (air as medium,  
59 frequency and voltage), due to its simple and versatile electrode geometry (planar or circular) and its  
60 ability to produce a stable discharge with negligible thermal effects (Tang et al., 2018). Moreover,

the separated configuration between electrodes and PAW limits corrosion phenomena, and avoids contamination of water with heavy metals easily occurring in underwater systems such as plasma jet devices, which are therefore unsuitable for food applications. Finally, the DBD plasma device is known to produce higher amount of active species with respect to plasma jet glow discharges (Leduc et al., 2010) due to its larger surface area. Reactive species are generated through collision mechanisms in the gas phase. When air is used as working gas to generate non-equilibrium plasma discharges, reactive oxygen species (ROS) and reactive nitrogen species (RNS) are formed. Ozone ( $O_3$ ), atomic oxygen ( $O$ ) and hydroxyl radical ( $OH^\bullet$ ) are the main ROS, while excited molecules of  $N_2$  and nitrogen oxide radicals are the main RNS characterizing a non-equilibrium plasma (Ragni et al., 2010). Many authors investigated reactions involving these species in gas phase (Du et al., 2008, Misra et al., 2016, Moreau et al., 2016, Yousfi et al., 2011) or in liquid phase for underwater devices (Lukes et al., 2012, Sun et al., 2012, Tian et al., 2014). However, the interaction of plasma generated in gas phase close to a liquid medium, and the distribution of active species in the liquid phase is less understood (Jiang et al., 2016), although this information is crucial to understand and control the decontamination capability of the system. Active species generated by the plasma discharge can directly diffuse through the gas/liquid interface, or can be generated in the liquid phase by post-discharge chemical reactions (Bruggeman et al., 2016, Zhou et al., 2018, 2016). The complexity of this scenario has been mainly approached by numerical simulation techniques which allowed to estimate mass transfer kinetic and other relevant parameters. For instance, numerical simulation performed by Yusupov et al. (2013) showed that ROS possessed high penetrating power into a 500 molecule thick water layer. Liu et al. (2016) investigated the role of the air gap between the plasma and the liquid medium and concluded that for gaps larger than 0.5 cm the concentration of active species in the PAW steeply decreases. In almost all the experimental investigations the pH value of the PAW reduces up to 3 - 3.5 after few minutes of discharge (Liu et al., 2010, Moreau et al., 2007). The concentration of reactive species in the liquid phase depends on several factors such as the system configuration, treatment time, discharge gap, carrier gas, applied voltage, and the electron energy

87 (Gurol et al., 2012, Pavlovich et al., 2013, Tian et al., 2015). In a recent review, it has been reported  
88 that ozone, hydrogen peroxide, nitrite, nitrate, superoxide ions, and peroxyxynitrite are the active  
89 species mainly present in PAW (Perinban et al., 2019).

90 Heterogeneous photocatalysis is one of the most studied advanced oxidation processes for  
91 environmental purposes (Parrino et al., 2019).  $\text{TiO}_2$  is widely used as the photocatalyst in these  
92 applications due to its low cost, non-toxicity, stability and high activity. Briefly, under irradiation of  
93 suitable wavelength, electrons and holes are generated in the conduction and valence bands of  $\text{TiO}_2$ ,  
94 respectively. Interfacial electron transfer with species adsorbed to or in proximity of the surface of  
95  $\text{TiO}_2$  induces formation of highly oxidizing radical species such as hydroxyl, superoxide, nitrate  
96 radicals and singlet oxygen (Parrino et al., 2018), which are mainly responsible for the degradation  
97 and mineralization of pollutants (Hamrouni et al., 2020) and for inactivation of pathogens such as  
98 bacteria, fungi, algae, viruses and microbial toxins (Kumar and Bansal, 2013, Zhu et al., 2018). In  
99 particular,  $\text{TiO}_2$  photocatalysis has been used for the disinfection of washing water coming from fresh  
100 vegetables industry towards natural microflora and potentially pathogenic microflora (Selma et al.,  
101 2008). Others research experiences refer about the bactericidal photocatalytic activity of  $\text{TiO}_2$  on  
102 carrots (Cho et al., 2007) and iceberg lettuce (Kim et al., 2007) with respect to both washing water  
103 and vegetables decontamination.

104  $\text{TiO}_2$  photocatalysis has been often integrated with other purification techniques such as biological  
105 treatments (Parrino et al., 2019b), adsorption onto activated carbons (Cataldo et al., 2016), ozonation  
106 (Camera-Roda et al., 2019), membrane separation (Toledano Garcia et al., 2018), among others.

107 Combination of cold plasma and photocatalysis is mainly reported for air purification systems. In  
108 these cases, synergistic effects between the two technologies have been observed, mainly justified by  
109 invoking the well-known synergy between  $\text{TiO}_2$  photocatalysis and ozone (Parrino et al., 2013). For  
110 instance, synergistic effects have been observed for the degradation of isovaleraldehyde (Palau et al.,  
111 2015) and butyraldehyde (Gharib-Abou et al., 2016) in gas phase. Coupled photocatalysis-plasma  
112 systems have been also applied for smoking rooms air deodorization (Ochiai et al., 2012), hospital

113 indoor air decontamination (Zadi et al., 2018), oxidation of mixtures of pollutants (Vorontsov et al.,  
114 2012), and reduction of CO<sub>2</sub> into CO and O<sub>2</sub> at low temperatures (Mei et al., 2016).  
115 On the other hand, only few researches deal with DBD plasma-photocatalysis systems for the  
116 decontamination of liquid media. In most of these applications the plasma discharge is generated  
117 underwater using point to plane geometry electrodes. The degradation of model pollutants such as  
118 phenol, 4-chlorophenol, or tetracycline occurred faster than the single processes in most of the cases  
119 when TiO<sub>2</sub> was suspended (He et al., 2014) or deposited on supports (Lukes et al., 2005). Similar  
120 results have been obtained in such systems also for the inactivation of E. Coli by using microplasma  
121 jet arrays and N<sub>2</sub>, He, O<sub>2</sub> and air as the working gases (Zhou et al., 2016b). Only few reports deal  
122 with the degradation of pollutants in liquid phase below the DBD plasma discharge acting in the head  
123 space. For instance, Aziz et al. (2018) coupled different oxidation processes with DBD plasma in a  
124 planar falling film reactor, and compared the integrated processes in terms of energy yield. Ghodbane  
125 et al. (2014) reported on the degradation of the anthraquinone dye Acid Blue 25 by using DC glow  
126 discharge and TiO<sub>2</sub> photocatalysis. However, in these reports the term synergy has been often used  
127 to indicate a general increase of efficiency with respect to photocatalysis or plasma, but not with  
128 respect to their sum. Moreover, as demonstrated by Camera Roda and Santarelli (2007) when synergy  
129 between two processes exists, it depends primarily on the ratio between the rate of the two processes  
130 operating separately under the same experimental conditions. This result, often disregarded, allowed  
131 in this work to clarify the problem of synergy between TiO<sub>2</sub> photocatalysis and DBD plasma in non-  
132 submerged systems, by rationally approaching the intensification problem.

133

## 134 **2. Material and methods**

135 Figure 1 schematically shows the discharge chamber. The external walls of the chamber were made  
136 of Pyrex in order to allow external irradiation as below detailed.

137

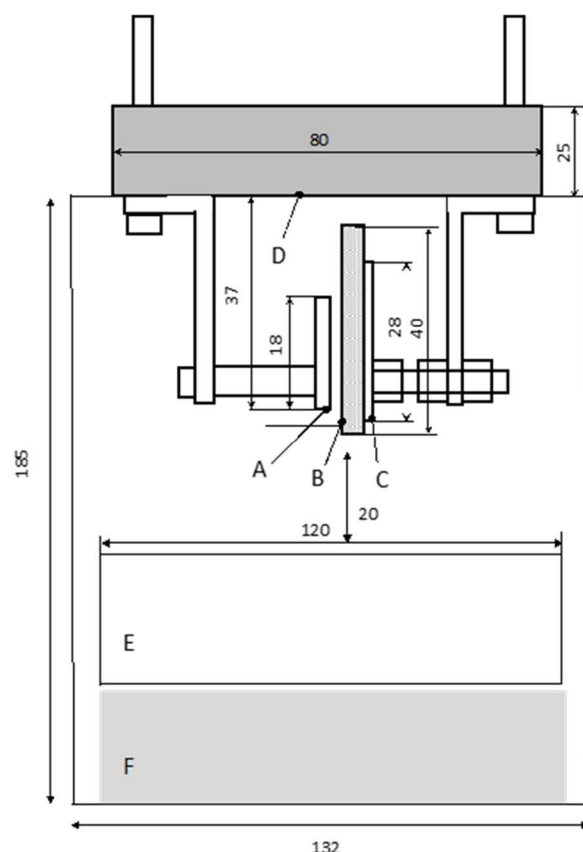


**Figure 1.** Layout of the discharge chamber. A: cathode; B: glass plate; C: anode; D: fan; E: Pyrex reactor; F: magnetic stirrer. The reported values of dimensions are in millimetres.

The degradation of methylene blue (MB, Sigma-Aldrich, St. Louis, Mo, USA) was used as model reaction to evaluate the decontamination efficiency of the system. 200 mL of magnetically stirred MB aqueous solution (0.02 mM, if not otherwise specified) was placed in a Pyrex cylindrical reactor (inner diameter 120 mm; height 60 mm) positioned within the chamber. The free surface of the solution was ca. 20 mm below the gas plasma discharge. The discharge was generated by using a dielectric barrier discharge (DBD) device characterized by two parallel plate electrodes made of brass ( $28 \times 12.6 \times 4.7$  mm) and stainless steel ( $18 \times 9.9 \times 5.5$  mm), respectively. The brass electrode was covered by a thin sheet of glass ( $40 \times 14.6 \times 0.05$  mm) working as dielectric barrier. Inside the chamber, a fan mounted at about 37 mm from the bottom of the stainless steel electrode was placed in order to direct the afterglow species towards the free surface of the methylene blue aqueous solution.

153 The discharge was driven by high voltage transformers and power switching transistors supplied by  
154 a stabilized DC power supply (Elektro-Automatik GmbH & Co.KG, Viersen, Germany, EA-PS 2042-  
155 06B) placed outside the chamber. Input voltage of 19.15 V ( $3.15 \pm 0.5$  A) and air as working gas were  
156 considered.

157 The voltage output was characterized by a like-shaped sinusoidal waveform with a peak to peak value  
158 of 13.8 kV (frequency around 46 kHz).

159 The concentration of MB during the treatments was measured by means of a Shimadzu UV-vis  
160 spectrophotometer (Kyoto, Japan) which measured the absorbance at 663 nm of samples withdrawn  
161 during the runs at fixed intervals of times. TiO<sub>2</sub> P25 (Evonik, Essen, Germany; specific surface area  
162  $56 \text{ m}^2 \cdot \text{g}^{-1}$ , 93% anatase, 7% rutile) was used as the photocatalyst for selected runs in amounts ranging  
163 from 0.01 to  $1 \text{ g} \cdot \text{L}^{-1}$  (Bellardita et al., 2017, 2018). Selected runs have been performed from 3 to 5  
164 times and the reproducibility was better than 5%.

165 Irradiation was performed by means of six actinic Mercury UV-A lamps (Philips, Eindhoven, The  
166 Netherlands; nominal power 14 W each, with emission peak at 365 nm) surrounding the chamber in  
167 a hexagonal geometry. The radiation intensity of each lamp was ca.  $7 \text{ W} \cdot \text{m}^{-2}$ , as measured at the  
168 reactor wall point nearest to the lamp by means of a Delta Ohm DO9721 radiometer equipped with a  
169 UVA probe. After 10 minutes of plasma treatment the temperature inside the glass chamber reached  
170  $33 \pm 1^\circ\text{C}$  (starting from ca.  $26^\circ\text{C}$ ) and was constant during the treatment. The chemical  
171 characterization of the atmosphere within the chamber in the presence of the discharge has been  
172 elsewhere reported (Ragni et al., 2016).

173 Tests to unveil the role of peroxyxynitrite and hydrogen peroxide have been performed according to the  
174 following procedures. Detection of H<sub>2</sub>O<sub>2</sub> in the reacting mixture was performed by the titanium  
175 peroxide method (Wolfe, 1962). Briefly, 5 mL of TiCl<sub>4</sub> (Sigma Aldrich, p.a.) were added to 5 mL of  
176 a 6M aqueous solution of HCl at ice temperature and then diluted to 500 mL in 6M HCl. Aliquots of  
177 this solution were added to the sample and the absorbance of the yellow titanium peroxo complex  
178 (measured by means of a Shimadzu UV-vis spectrophotometer, Jasco V-570, Japan) was used to



check the presence of hydrogen peroxide. Peroxynitrite standard solutions were prepared by mixing 1 mL of sodium nitrite (0.3 M, Sigma Aldrich, p.a.), 1 mL hydrogen peroxide (0.7 M, Sigma Aldrich, p.a.) and 0.5 mL of hydrochloric acid (0.6 M, Sigma Aldrich, 37%) as aqueous solutions. 0.5 mL of an aqueous solution of sodium hydroxide (1.5 M, Sigma Aldrich, p.a.) was immediately added within 2-3 seconds to stabilize the solution. Nitrite ion was the limiting reactant, and to eliminate the excess of H<sub>2</sub>O<sub>2</sub>, the solution was mixed with MnO<sub>2</sub> (Sigma Aldrich p.a.), left under stirring for 20 minutes, and filtered. MB was added to the solution and the pH was adjusted to ca. 2 by adding HCl. Finally, the solution was kept in the dark for 20 minutes and irradiated under UVA light (10 W UV LED, supplied by GraceLightLed) for 5 minutes. The concentration of MB during the tests was measured by UV-vis spectroscopy (Jasco V-570, Japan). Benzoic acid (Sigma-Aldrich, p.a.) has been used as a molecular trap to highlight the presence of hydroxyl radicals in the reacting mixture, by monitoring the formation of salicylic acid through fluorescence spectroscopy ( $\lambda_{exc}$ = 270 nm, Jasco FP-6300, Japan).

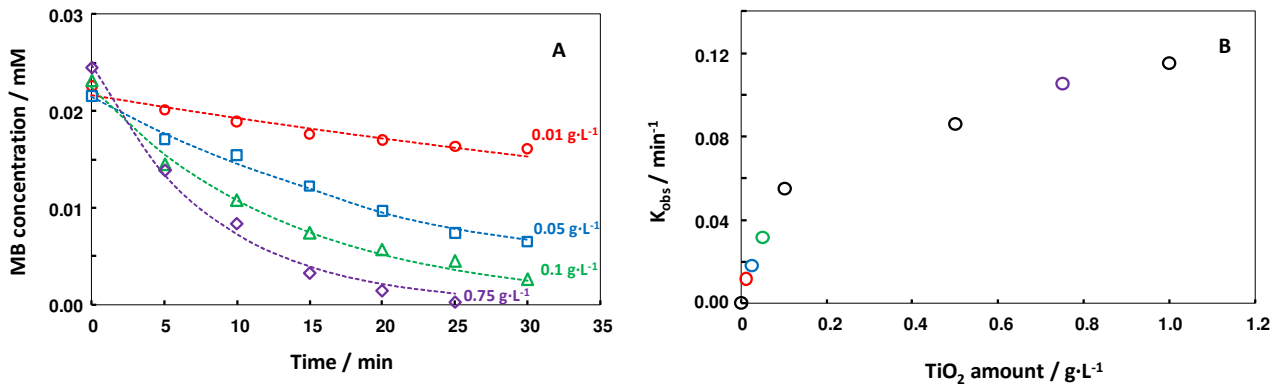
### 3. Results and discussion

Preliminary photocatalytic experiments were carried out at a fixed initial MB concentration by changing the amount of TiO<sub>2</sub> and keeping constant the other experimental conditions. Results are represented by symbols in Figure 2A. Experimental data have been fitted by using Eq. 1, as the photocatalytic degradation of MB proceeds according to first order kinetics (Salehi et al. 2012).

$$r = -\frac{dC_{MB}}{dt} = k_{obs}C_{MB} \quad (1)$$

where  $r$  is the reaction rate,  $C_{MB}$  the concentration of MB, and  $k_{obs}$  the observed apparent kinetic constant. The values of the initial MB concentration and of  $k_{obs}$  have been obtained by fitting the experimental concentration vs. time data by the least squares method. As it is evident the model satisfactorily fits the experimental data. The obtained values of  $k_{obs}$  are reported in Figure 2B against the TiO<sub>2</sub> amount suspended in the photocatalytic medium.

204



205

206 **Figure 2.** MB photocatalytic degradation during irradiation time, for some representative runs carried  
 207 out in the presence of different concentrations of TiO<sub>2</sub> (Panel A). The observed kinetic constants have  
 208 been reported in Panel B against the amount of TiO<sub>2</sub> dispersed in the photocatalytic medium.

209

210 A linear behavior of the observed kinetic constant (see Eq. 1) for the photocatalytic reaction rate  
 211 against the photocatalyst amount is apparent up to TiO<sub>2</sub> concentrations of ca. 0.1 g·L<sup>-1</sup> (see Panel B),  
 212 while the curve tends to a plateau for higher TiO<sub>2</sub> amounts. The mechanism of the photocatalytic  
 213 degradation of MB is well known, and readers are referred to the relevant literature for details (Dariani  
 214 et al. 2016). Briefly, irradiating TiO<sub>2</sub> under UV light results in the formation of electron-hole pairs  
 215 (Eq. 2). Highly oxidizing hydroxyl radicals, formed upon reduction of oxygen (Eq. 3-5) and water  
 216 oxidation (Eq. 6), along with other reactive oxygen species (ROS) such as singlet oxygen (Eq. 7)  
 217 (Parrino et al., 2018) are, in turn, mainly responsible for the degradation of MB.

218



225

226 We would like to stress here that the use of dyes should be avoided in photocatalysis when testing  
227 novel photocatalysts under visible light irradiation (Yan et al., 2006). In fact, the complex  
228 photochemistry of MB (Mitoraj et al. 2018) and the substrate dependent nature of photocatalysis (Ryu  
229 and Choi, 2008, Parrino et al. 2017) could produce results of difficult interpretation. Moreover,  
230 indirect photocatalytic mechanisms triggered by the excited triplet state of the dye could mask the  
231 real activity of the photocatalytic material. In this case, however,  $\text{TiO}_2$  is the main light absorbing  
232 species due to the fact that the irradiation wavelength (centered at 365 nm) matches its absorption  
233 band, and that at this wavelength range MB shows low absorption capability. Therefore, indirect  
234 photocatalytic paths can be neglected in these conditions. Accordingly, blank tests performed by  
235 irradiating MB solutions in the absence of  $\text{TiO}_2$  did not result in appreciable MB degradation within  
236 the considered time range.

237 In order to investigate the coupling between plasma treatment and photocatalysis, we performed the  
238 photocatalytic degradation of MB under external UV light irradiation and in the presence of  $\text{TiO}_2$ , by  
239 simultaneously switching on the plasma discharge within the system. Results are represented in  
240 Figure 3 by the curve labelled as PL@PC@UV. Figure 3 reports also the MB degradation due to the  
241 sole photocatalysis (PC@UV curve) and to the plasma treatment under simultaneous UV light  
242 irradiation (PL@UV curve). Notably, all of the three runs reported in Figure 3 have been carried out  
243 under UV irradiation, for the sake of comparison.

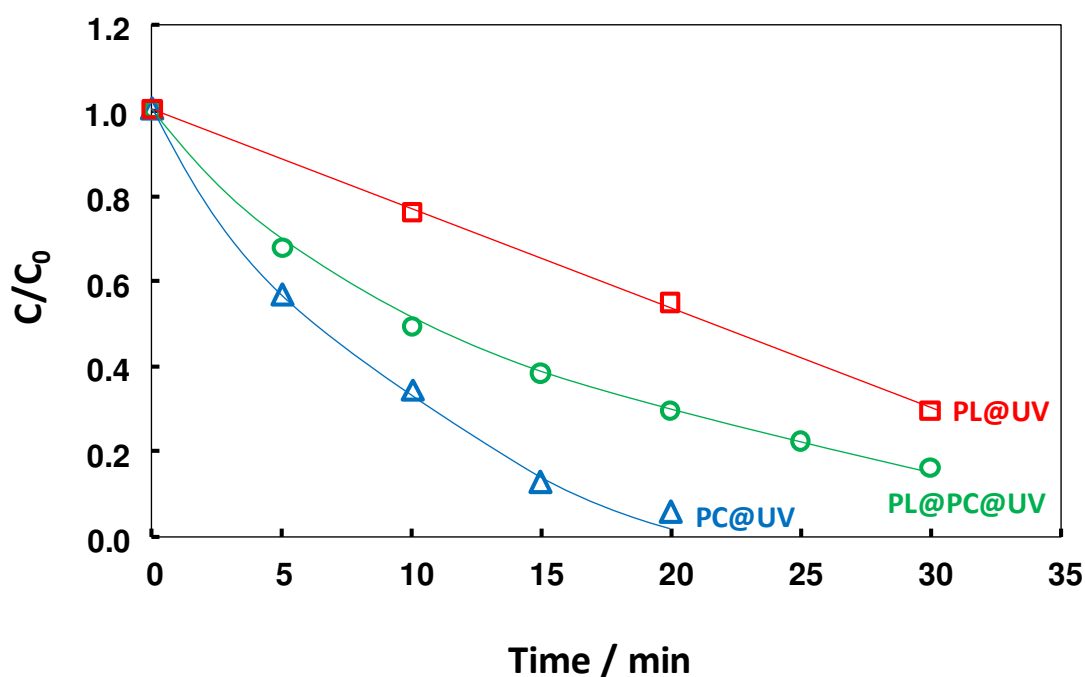


**Figure 3.** Normalized concentration of MB during reaction time for some representative runs of sole photocatalysis (PC@UV, blue triangles), plasma-UV (PL@UV, red squares), and plasma-photocatalysis (PL@PC@UV, green circles). Initial MB concentration  $C_0 = 0.02$  mM,  $\text{TiO}_2$  amount for the photocatalytic runs  $0.75 \text{ g}\cdot\text{L}^{-1}$ .

Under the given experimental conditions, the degradation rate of MB due to the sole photocatalysis is faster than the one induced by plasma and UV light. However, surprisingly, the MB degradation obtained when coupling plasma and photocatalysis is slower than that of photocatalysis alone, even if it is higher with respect to that of plasma and UV light. This implies that in this case the two technologies not only do not show any synergistic effect, but the simultaneous use of plasma and photocatalysis is detrimental with respect to the sole photocatalysis.

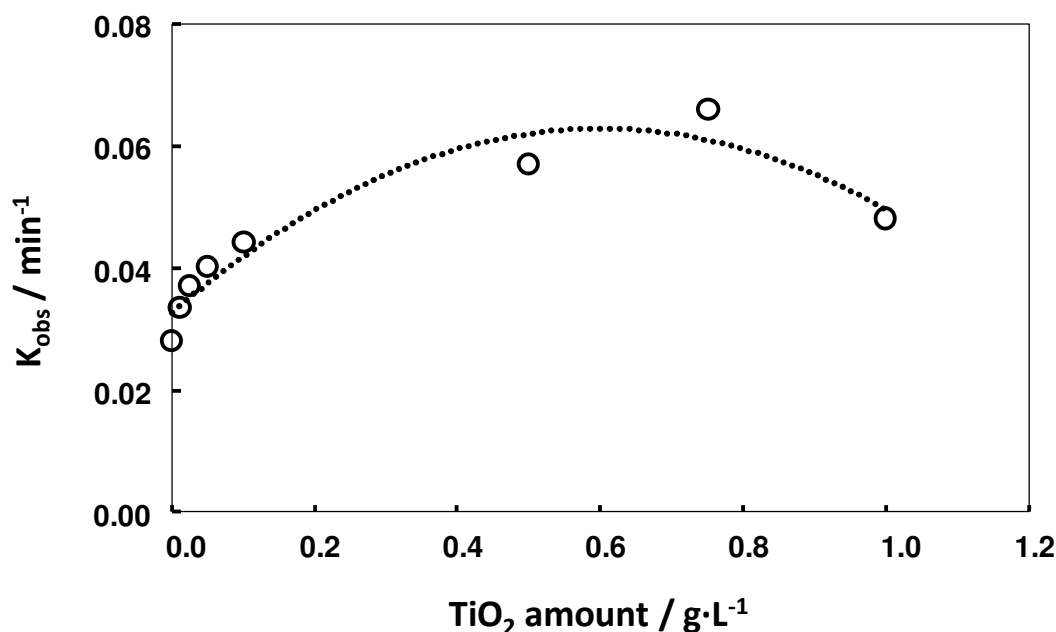
These results do not agree with those reported in literature in which, generally, the integration of plasma and photocatalysis results in process intensification. It is worth mentioning that low energy DBD plasma has been poorly investigated in literature and integration with photocatalysis has been carried out in gas phase but never in the head space above a photocatalytic liquid suspension as in this case. The reported synergy between plasma and photocatalysis for the degradation of model

compounds in gas phase, such as butyraldehyde and isovaleraldehyde, (Palau et al., 2015, Gharib-Abou et al., 2016) has been justified by assuming that the ozone produced by plasma was the main oxidant, and that its concomitant action with the irradiated TiO<sub>2</sub> increased the degradation rate with respect to the sum of the single technologies (Camera-Roda et al., 2017). In fact, in the presence of ozone only 1 electron (1 photon) is required to produce one OH radical (Eq. 8-9), while 3 electrons (3 photons) are necessary in the presence of oxygen (Eq. 3-5).



The evident absence of synergy expressed in Figure 3 can be due to different reasons. First of all, the diffusion of ozone from the gas phase (where it is generated) to the liquid phase could limit the process. The ozone diffusion coefficient has been estimated by Jiang et al. (2013) being  $1.75 \cdot 10^{-5} \text{ cm}^2 \cdot \text{s}^{-1}$ . Ozone can effectively oxidize MB at the gas-liquid interface or even within the first liquid layers, but its action can be limited by mass transfer within the bulk of the solution. Notably, in the present experimental set up only gentle magnetic agitation could be performed, as at higher agitation speeds formation of water droplets within the electrodes destabilized the discharge. As demonstrated in the relevant literature (Parrino et al., 2013), the synergy between photocatalysis and ozone is dependent on the ratio between the rates of the single technologies. This aspect is generally disregarded, whereas it might explain why in some cases the values of the intensification factors measured by different researchers are very dissimilar. Therefore, in principle, opposite results could be obtained also in this case by changing the rate of one of the two processes. In order to check this hypothesis, we measured the MB degradation rate in the plasma-photocatalysis integrated system at different TiO<sub>2</sub> concentrations. The apparent observed kinetic constants were determined differentiating the experimental data at the initial time, by using a five points formula for equally

286 spaced points (Yeow et al., 2003, Lubansky et al., 2006). The obtained  $k_{\text{obs}}$  values versus the amount  
 287 of  $\text{TiO}_2$  for the plasma-photocatalysis integrated process are reported in Figure 4.



288

289

290 **Figure 4.** Observed kinetic constants calculated at the initial time against the amount of  $\text{TiO}_2$   
 291 for integrated runs with plasma and photocatalysis.

292

293 It is apparent that the initial rate of degradation of MB, proportional to the  $k_{\text{obs}}$  values, during the  
 294 coupled plasma-photocatalytic process increases with the amount of photocatalyst until a maximum  
 295 is reached. Thereafter, for  $\text{TiO}_2$  concentrations higher than ca.  $0.5\text{-}0.7 \text{ g}\cdot\text{L}^{-1}$  the rate of the integrated  
 296 process decreases. The presence of a maximum indicates the existence of an optimum at which  
 297 photocatalysis and plasma can be used at the highest efficiency. On the other hand, such a behavior  
 298 is the typical result of two contrasting processes operating simultaneously during the integrated  
 299 process. As above reported (Figure 2B) the rate of photocatalysis increases until a plateau is reached.  
 300 Therefore, a second process, related to the plasma discharge and/or with UV light irradiation, must  
 301 contribute to MB degradation and its efficiency is supposed to decrease with increasing catalyst  
 302 loading.

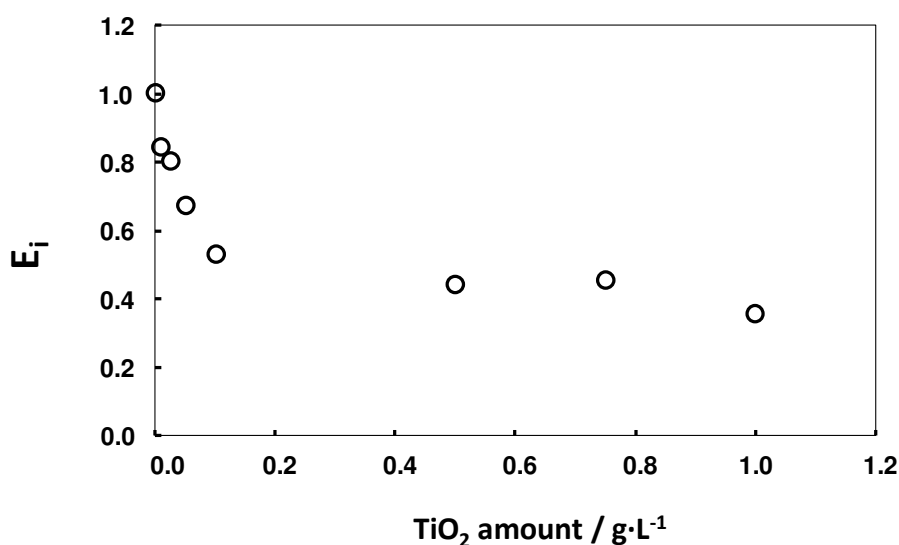
303 In order to evidence the nature of this second process, it is useful to define the following integration  
 304 factor ( $E_i$ ) as in Eq. 10

305

$$306 \quad E_i = \frac{k_{obs}(PC@PL@UV)}{k_{obs}(PC@UV) + k_{obs}(PL@UV)} \quad (10)$$

307

308 Where  $k_{obs}(PC@PL@UV)$  is the observed rate constant of the integrated plasma-photocatalysis  
 309 process, while  $k_{obs}(PC@UV) + k_{obs}(PL@UV)$  is the algebraic sum of the rate constants of  
 310 photocatalysis and plasma-UV processes. In other words,  $E_i$  expresses at which extent the integrated  
 311 process is more (if  $E_i > 1$ ) or less effective (if  $E_i < 1$ ) with respect to the sum of the two processes  
 312 acting separately. In Figure 5 is reported the trend of the integration factor ( $E_i$ ) at increasing  $TiO_2$   
 313 amounts.



314

315 **Figure 5.** Trend of the integration factor  $E_i$  at increasing concentration of  $TiO_2$

316

317 In the absence of photocatalysts,  $E_i$  is equal to 1 by definition. By increasing the amount of  $TiO_2$ , the  
 318 integrated process is progressively less efficient than the sum of the two processes until, at a  $TiO_2$   
 319 concentration of ca.  $0.2 \text{ g} \cdot \text{L}^{-1}$ , a plateau is reached. Two conclusions can be drawn from these results:  
 320 (i) a negative synergy is observed between plasma and photocatalysis under these conditions; (ii) the

321 ozone induced oxidation process, known to provide a positive synergy when coupled with  
322 photocatalysis, plays a minor role when photocatalysis acts together with DBD plasma.

323 The detrimental effect of  $\text{TiO}_2$  on the plasma induced MB degradation is necessarily due to the  
324 interaction between  $\text{TiO}_2$  and some species generated by the discharge which then dissolve in the  
325 reacting suspension. In this regard, it should be noted that the pH of the solution changed from around  
326 6 to 3 within the first 15 minutes of discharge and UV-vis spectra of the solutions showed the presence  
327 of nitrate and nitrite ions according to literature (Ragni et al., 2016).

328 Blank photocatalytic tests of MB degradation performed in the presence of nitrate and nitrite ions,  
329 while maintaining constant the other conditions, did not show significant differences, indicating that  
330 these ions, generated upon the plasma discharge, are not directly responsible for the observed  
331 behavior. Regardless of their nature, the oxidizing species produced by the plasma discharge are  
332 deactivated by the presence of  $\text{TiO}_2$ . This can occur by interaction of these species with the  
333 photogenerated charges at the surface of  $\text{TiO}_2$ , or simply because  $\text{TiO}_2$  acts as UV light screen, thus  
334 reducing their direct photochemical activation. If the second hypothesis holds, the extent of the effect  
335 of plasma during photocatalysis should be dependent on the portion of the reactor effectively  
336 irradiated. In fact, the higher is the concentration of  $\text{TiO}_2$ , the lower is the penetration of the light and  
337 the smaller is the volume of the reactor where irradiation is effective.

338 To tackle this issue, for each photocatalyst concentration we calculated the mean free photonic path  
339 (i.e. the radius of the reactor annulus well irradiated, at which the optical thickness is equal to 1) as  
340 the ratio between the radius of the reactor and the optical thickness. Note that the optical thickness is  
341 equal to the specific extinction coefficient of  $\text{TiO}_2$  P25 at 365 nm ( $5.8 \cdot 10^4 \text{ cm}^2 \cdot \text{g}^{-1}$ ) multiplied by the  
342 photocatalyst concentration and by the radius of the reactor (Satuf et al., 2005). In this way it is  
343 possible to estimate the percentage of the photoreactor effectively irradiated ( $\%V_{\text{irr}}$ ) at each  
344 photocatalyst concentration. Results are reported in Figure 6.

345



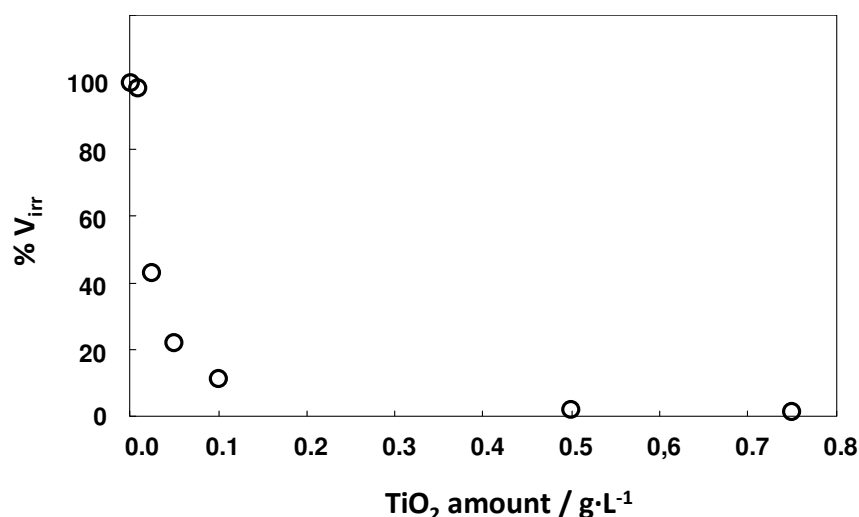


**Figure 6.** Percentage of reactor volume effectively irradiated at different TiO<sub>2</sub> concentrations of the suspension.

Results show that in the absence of the photocatalyst the whole volume is effectively irradiated ( $\%V_{irr} = 100$ ), while increasing the photocatalyst concentration results in a steep decrease of the portion of volume effectively irradiated until, for TiO<sub>2</sub> amounts higher than ca. 0.2 g·L<sup>-1</sup>, the decrease is negligible and a plateau is reached. It is evident that while the rate of photocatalysis reaches a plateau for TiO<sub>2</sub> concentrations higher than 0.75 g·L<sup>-1</sup> (Figure 2B), the trend of the integration factor  $E_i$  (Figure 5) is similar to that of the percentage of volume well irradiated (Figure 6), as it reaches a plateau at ca. 0.2 g·L<sup>-1</sup>. This evidence supports the hypothesis that TiO<sub>2</sub> simply acts as a screen during the integrated plasma-photocatalysis process and that some of the photoactive species produced by the discharge are simply activated by UV light.

As a further proof of the existence of UV light absorbing species generated by the plasma discharge and contributing to MB degradation, we performed the plasma treatment in the absence of TiO<sub>2</sub>, with and without UV light irradiation. Results are shown in Figure 7.

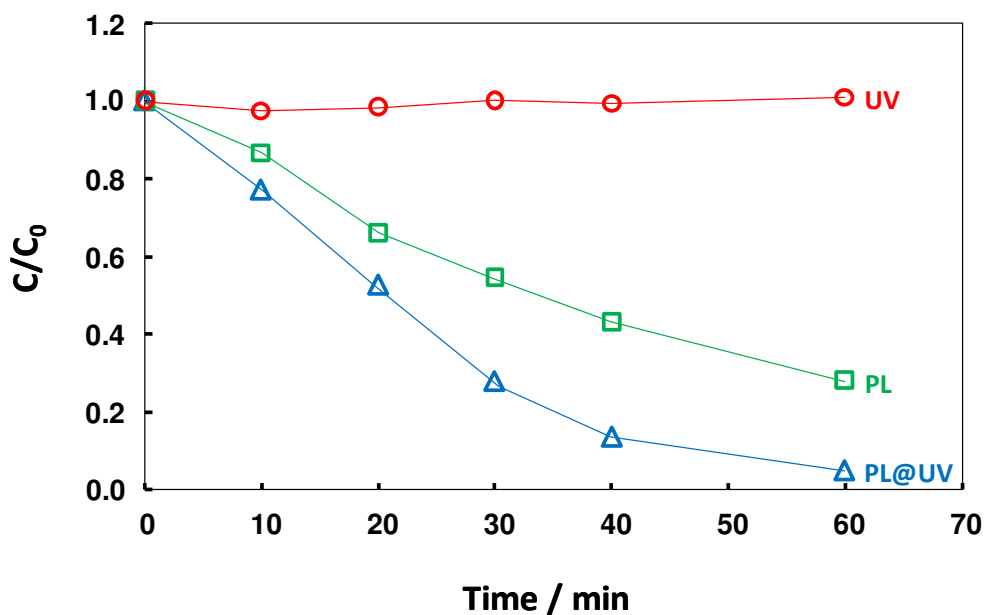
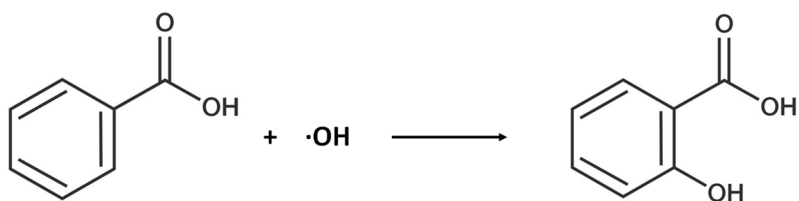


**Figure 7.** Normalized concentration of MB during time for runs performed under sole UV light irradiation (red circles, UV), by the sole plasma discharge treatment (green squares, PL), and by plasma discharge treatment performed under simultaneous UV light irradiation (blue triangles, PL@UV).

It is evident that UV light alone does not induce MB degradation. Contrarily, plasma discharge in the absence of external UV light irradiation results in ca. 40% degradation of MB after 30 minutes of irradiation, while the degradation reached ca. 70% in the same time when the solution is externally irradiated. This result confirms that the plasma discharge produces species that are activated by UV light. To unravel the mechanism underlying this effect, we checked the presence of OH radicals in the irradiated and non-irradiated suspensions in the presence of the plasma discharge. We perform the experiments by only substituting MB with benzoic acid, under otherwise identical conditions. In fact, in the presence of OH radicals, benzoic acid is hydroxylated to salicylic acid according to Eq. 11.



(11)

The presence of salicylic acid has been detected by measuring its fluorescence at 410 nm. Results are shown in Figure 8.

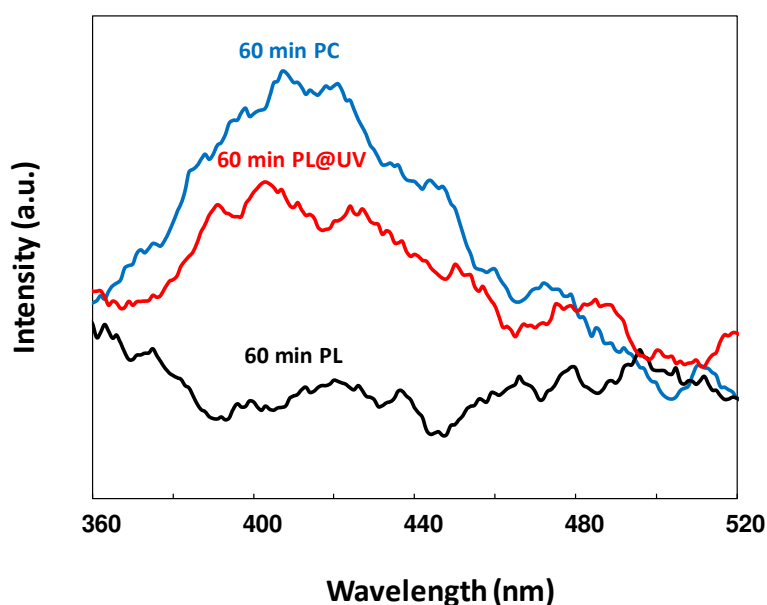


**Figure 8.** Fluorescence spectra of samples of reacting suspension for runs carried out in the presence of 0.5 mM of benzoic acid after 60 minutes of plasma treatment (black curve), of plasma under external UV light irradiation (red curve), and of photocatalytic treatment without plasma and with 0.1 g·L<sup>-1</sup> TiO<sub>2</sub> (blue curve). Excitation wavelength: 270 nm.

Notably, a quantitative comparison of the spectra was not possible due to the influence of the different treatments on the composition of the suspension. However, it can be seen that salicylic acid could be detected in the presence of irradiated TiO<sub>2</sub> (blue curve), and in the presence of the plasma discharge, only if the solution was externally irradiated. On the contrary, salicylic acid was virtually absent when the plasma treatment was performed under dark conditions.

393 Formation of hydroxyl radicals by means of photocatalysis is well documented and occurs according  
394 to Eqs. 2-6.

395 The absence of hydroxyl radicals when the solution was treated by plasma under dark conditions is  
396 reasonable, by considering that hydroxyl radicals eventually formed in the discharge zone could not  
397 live enough to reach the bulk of the solution beneath. In fact, the life time of OH radicals is reported  
398 to be in the order of magnitude of microseconds (Perinban et al., 2019).

399 On the other hand, when plasma discharge was performed under external UV irradiation, the  
400 formation of salicylic acid could be detected, thus indicating that hydroxyl radicals are responsible  
401 for the enhanced MB degradation observed when plasma was performed under UV irradiation with  
402 respect to the dark conditions.

403 This finding justifies the previously observed detrimental behaviour of TiO<sub>2</sub> when plasma and  
404 photocatalysis simultaneously operated. In fact, photochemical reactions triggered by UVA light  
405 absorbing species must be the responsible for the observed formation of hydroxyl radicals.

406 Direct detection of these species was not straightforward at this step of research, by considering their  
407 possible transient nature. However, some hypotheses can be proposed, while further investigation are  
408 ongoing to afford definitive proofs.

409 OH radicals could form from hydrogen peroxide (Cataldo, 2014) which undergo photolysis at any  
410 wavelength lower than 380 nm with a quantum yield  $\Phi$  ranging between 1 and 1.5, according to Eq.  
411 12.

412



414

415 However, during plasma treatment the amount of H<sub>2</sub>O<sub>2</sub> in the liquid phase was lower than the  
416 detection limit (1  $\mu\text{M}$ ) of the method based on titanium peroxocomplexes described in the  
417 experimental part. On the other hand, as the absence of evidence is not evidence of absence, it cannot  
418 be excluded that hydrogen peroxide could be present at lower concentrations or for times shorter than

those of analysis. In fact, the presence of hydrogen peroxide has been often reported in similar systems, even if at concentrations closer to the detection limit (Ragni et al., 2016).

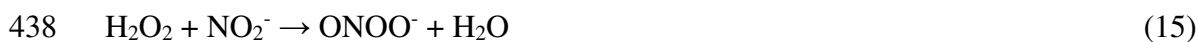
Nitrate ions photolysis could be excluded as a source of hydroxyl radicals as photons below 300 nm (required for this reaction) are cut off by Pyrex glass (Parrino et al., 2016).

The presence of nitrite ions in solution with MB under UV irradiation did not result in MB degradation. Therefore, nitrite ions alone are not responsible for the observed production of hydroxyl radicals.

Peroxynitrite ion is reported among the species that can be present in the aqueous phase below the plasma discharge (Tarabová et al., 2019). Peroxynitrite ( $\text{ONOO}^-$ ) can be formed by reaction of superoxide and nitric oxide radicals (Eq. 13) formed after glow (Goldstein and Merényi, 2008). Notably the life time of the superoxide radical is long enough (ca. 5 seconds) in aqueous solution and is easily protonated to hydroperoxyl radical at pH lower than 4.8 (Eq. 14) (Bielski et al., 1985).



Moreover, peroxynitrite can be formed by reaction of nitrite and hydrogen peroxide according to Eq. 15 (Saha et al., 1998).



By considering that the pH of the MB solution is acidic (ca. 3), it is probable that peroxynitrite is present in its protonated form in solution. In fact, pKa of peroxynitrous acid is ca. 6.8. Peroxynitrous acid is a highly oxidizing and nitrating agent. It is rather unstable with respect to its corresponding anion, and it easily undergoes homolytic rupture to  $\text{NO}_2$  and hydroxyl radical. By considering that the peroxynitrite shows an absorption band with a maximum at 302 nm which can extends up to 390

445 nm, it is possible that production of hydroxyl radicals could be sped up under UVA irradiation.

446 Coddington et al. (1999) report the formation of hydroxyl radicals by decomposition of peroxyxynitrite

447 ions in aqueous solution. Beckman et al. (1990) observed that peroxyxynitrite rapidly decomposes once

448 protonated with a half-life of 1.9 s at pH 7.4 thereby generating a strong oxidant with reactivity similar

449 to hydroxyl radical. Khan et al. (2000) reported the decomposition of peroxyxynitrite to nitroxyl anion

450 and singlet oxygen. However, Martinez et al. (2000) soon later observed that formation of singlet

451 oxygen could be observed only in the presence of traces of hydrogen peroxide. Most of the reports

452 concern the behaviour of peroxyxynitrite under dark conditions, while few is known about its

453 photochemical behaviour. Recently Thøgersen et al. (2015) investigated the primary photochemistry

454 of peroxyxynitrite aqueous solutions irradiated at 266 nm by transient absorption spectroscopies. More

455 than 90% of the peroxyxynitrite was dissociated after 400 ps and the dominant path was the formation

456 of superoxide anion radical and nitrogen monoxide. To the best of our knowledge the effects of

457 radiation at longer wavelengths have been poorly investigated. To the aim of our work, it was

458 interesting to ascertain if UVA irradiation could affect the degradation of MB in the presence of

459 peroxyxynitrite ions and/or hydrogen peroxide. Further investigation is ongoing in order to detail the

460 mechanistic aspects of this behaviour.

461 Figure 9 shows the normalized concentration of MB under dark and under UVA irradiation in the

462 presence and in the absence of peroxyxynitrite ions. Notably, the pH of the as prepared standard solution

463 was ca. 12. Blank tests allowed to determine that MB degradation, at this pH value, proceeded both

464 under dark conditions and (faster) under UVA irradiation even in the absence of peroxyxynitrite.

465 Therefore, the tests in Figure 9 have been performed by acidifying the solution containing MB at pH

466 ca. 3 (i.e. the pH of the MB solution under plasma discharge) by means of HCl (0.7 M solution)

467 addition prior to starting the test.

468

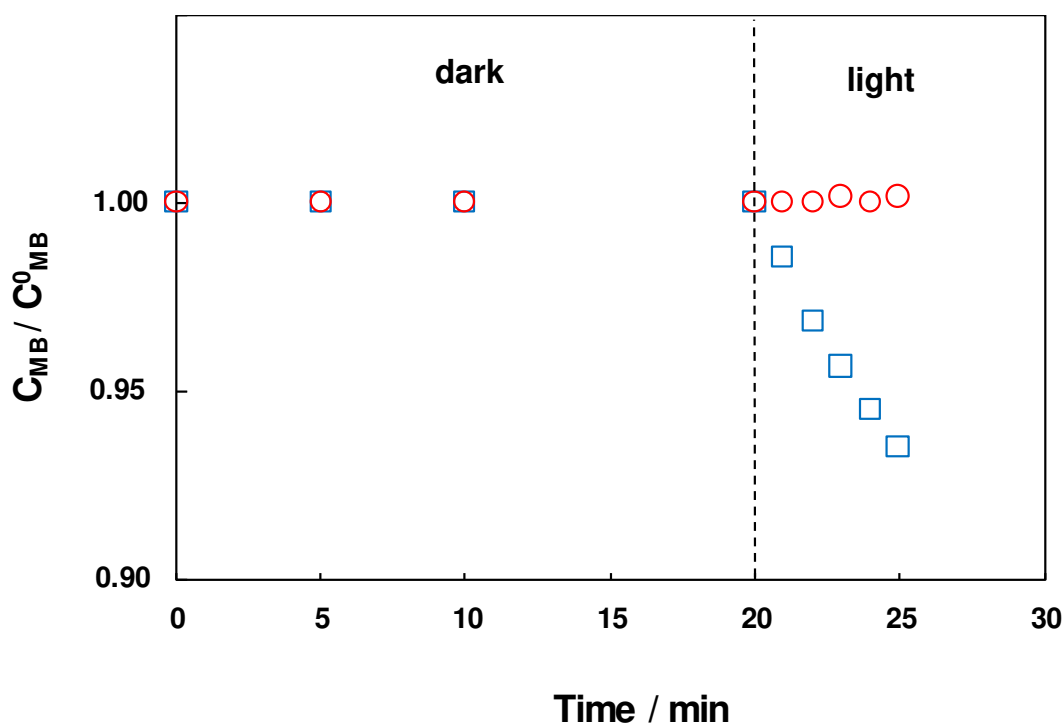


**Figure 9.** Normalized concentration of MB versus time in acidified (pH = 3) peroxynitrite standard solution (blue squares) and in the absence of peroxynitrite (red circles) under dark and under UV light irradiation.

Addition of HCl resulted in an immediate drop of MB concentration, possibly due to direct peroxynitrous acid formation that induced oxidation (not shown in Figure 9). Thereafter, the MB concentration was stable under dark and the pH was constant at ca. 3. The solution was maintained in the dark for twenty minutes and the concentration of MB did not decrease as it is evident from Figure 9. However, under UVA irradiation the concentration of MB decreased of ca. 8% after 5 minutes in the presence of peroxynitrite, while remained constant in its absence.

Blank tests performed in the absence of peroxynitrite but in the presence of H<sub>2</sub>O<sub>2</sub> afforded similar results (not shown). Even if hydrogen peroxide was removed from the peroxynitrite solution by passing it through powdered MnO<sub>2</sub>, and its concentration was monitored by the titanium peroxide method, the presence of H<sub>2</sub>O<sub>2</sub> at concentration lower than the detection limit cannot be excluded in the present experimental conditions. However, the present tests suggest that peroxynitrite and/or

485 hydrogen peroxide could be tentatively proposed as the active species responsible for the enhanced  
486 MB degradation observed when plasma discharge acts under UVA irradiation.

487

#### 488 **4. Conclusions**

489 The interaction between photocatalysis and the plasma discharge generated above the liquid  
490 suspension by means of a DBD device, has been investigated by monitoring the degradation of  
491 methylene blue in the aqueous phase as a model reaction. Results showed an optimum in the  
492 efficiency of MB degradation obtained by coupling plasma and photocatalysis exists for  $\text{TiO}_2$   
493 concentrations of ca.  $0.5 \text{ g}\cdot\text{L}^{-1}$ . This bell behaviour, however, indicates the existence of two  
494 contrasting processes simultaneously acting during the integrated process. In fact, increasing the  
495 amount of  $\text{TiO}_2$  results in higher photocatalytic activity but, at the same time is detrimental as far as  
496 the joint effect of plasma and photocatalysis is concerned. In fact, the efficiency of the integrated  
497 process with respect to the sum of the two processes acting separately decreases with increasing the  
498  $\text{TiO}_2$  concentration in the reacting mixtures. This finding has been related with the production of  
499 active species absorbing UVA light which in turn generate hydroxyl radicals in the aqueous solution,  
500 as demonstrated by fluorescence spectroscopy. Accordingly, in the absence of  $\text{TiO}_2$ , irradiating the  
501 aqueous solution above which the plasma is glowed enhances the degradation rate of MB with respect  
502 to the simple use of plasma. Experimental results show that peroxynitrous acid and/or hydrogen  
503 peroxide generated upon the action of plasma could be responsible for the observed behaviour.  
504 Notably, due to the substrate dependent nature of photocatalytic reactions, further investigation in the  
505 presence of different pollutants is required to obtain a full picture of the complex interplay between  
506 plasma and photocatalysis. However, these preliminary results define the terms of interaction between  
507 plasma and photocatalysis and show that the integration of these technologies under opportune  
508 conditions could be a promising alternative to the use of chlorine for the disinfection of fresh cut  
509 vegetables in the food processing chain.

510



511 **Competing interest statement**

512 The authors have no competing interests to declare.

513

514 **References**

515 Aziz, K.H.H., Miessner, A., Müller, H., Mueller, S., Kalass, D., Khorshid, I., Rashid, M.A.M., 2018.  
516 Application of a planar falling film reactor for decomposition and mineralization of methylene blue  
517 in the aqueous media via ozonation, Fenton, photocatalysis and non-thermal plasma: A comparative  
518 study. *Process Saf. Environ. Prot.* 113, 319-329. <https://doi.org/10.1016/j.psep.2017.11.005>

519 Barbosa-Cánovas, G.V., Donsi, F., Pokhrel, P.R., Candoğan, K., Guadarrama-Lezama, A.Y., 2017.  
520 Nonthermal stabilization processes, in: Roos, Y.H., Livney, Y.D. (Eds.), *Engineering Foods for*  
521 *Bioactives Stability and Delivery*, Springer, New York, pp. 341–360.

522 Beckman, J.S., Beckman, T.W., Chen, J., Marshall, P.A., Freeman, B.A., 1990. Apparent hydroxyl  
523 radical production by peroxynitrite: Implications for endothelial injury from nitric oxide and  
524 superoxide. *Proc. Natl. Acad. Sci. USA.* 87, 1620-1624. <https://doi.org/10.1073/pnas.87.4.1620>

525  
526 Bellardita, M., El Nazer H.A., Loddo V., Parrino F., Venezia A.M., Palmisano, L., 2017.  
527 Photoactivity under visible light of metal loaded TiO<sub>2</sub> catalysts prepared by low frequency ultrasound  
528 treatment. *Catal. Today* 284, 92–99. <http://dx.doi.org/10.1016/j.cattod.2016.11.026>

529  
530 Bellardita, M., Di Paola, A., Megna, B., Palmisano, L., 2018. Determination of the crystallinity of  
531 TiO<sub>2</sub> photocatalysts. *J. Photochem. Photobiol. A: Chem.* 367, 312-320.  
532 <https://doi.org/10.1016/j.jphotochem.2018.08.042>

533  
534 Berardinelli, A., Pasquali, F., Cevoli, C., Trevisani, M., Ragni, L., Mancusi, R., Manfreda, G., 2016.  
535 Sanitisation of fresh-cut celery and radicchio by gas plasma treatments in water medium. *Postharvest*  
536 *Biol. Technol.* 111, 297–304. <https://doi.org/10.1016/j.postharvbio.2015.09.026>

537  
538 Bhilwadikar, T., Pounraj, S., Manivannan, S., Rastogi, N.K., Negi, P.S., 2019. Decontamination of  
539 microorganisms and pesticides from fresh fruits and vegetables: a comprehensive review from  
540 common household processes to modern techniques. *Comp. Rev. Food Sci. F.* 18, 1003-1038.  
541 <https://doi.org/10.1111/1541-4337.12453>

542  
543 Bielski, B.H.J., Cabelli, D.E., Arudi, R.L. Ross, A.B., 1985. Reactivity of HO<sub>2</sub>/O<sub>2</sub><sup>-</sup> Radicals in  
544 Aqueous Solution, *J. Phys. Chem. Ref. Data* 14, 1041-1100. <https://doi.org/10.1063/1.555739>

545  
546 Bruggeman, P.J., Kushner, M.J., Locke, B.R., Gardeniers, J.G.E., Graham, W.G., Graves, D.B.,  
547 Ceriani, E., 2016. Plasma–liquid interactions: A review and roadmap. *Plasma Sources Sci. T.* 25,  
548 053002. <https://doi.org/10.1088/0963-0252/25/5/053002>

549  
550 Camera-Roda, G., Loddo, V., Palmisano, L., Parrino, F., 2019. Photocatalytic ozonation for a  
551 sustainable aquaculture: A long-term test in a seawater aquarium. *App. Catal. B: Environ.* 253, 69-  
552 76. <https://doi.org/10.1016/j.apcatb.2019.04.048>

553

554 Camera-Roda, G., Loddo, V., Palmisano, L., Parrino, F., Santarelli, F., 2017. Process intensification  
 555 in a photocatalytic membrane reactor: Analysis of the techniques to integrate reaction and separation,  
 556 Chem. Eng. J. 310, 352-359. <https://doi.org/10.1016/j.cej.2016.06.019>  
 557

558 Camera-Roda, G., Santarelli, F., 2007. Intensification of water detoxification reactors made easy by  
 559 considering the photons as immaterial reactants. J. Sol. Energy Eng. 129, 68–73.  
 560 <https://doi.org/10.1115/1.2391204>

561 Cataldo, F., 2014. Hydrogen peroxide photolysis with different UV light sources including a new  
 562 UV-LED light source. NEW FRONT. CHEM. 23, 99-110.

563 Cataldo, S., Ianni, A., Loddo, V., Mirenda, E., Palmisano, L., Parrino, F., Piazzese, D., 2016.  
 564 Combination of advanced oxidation processes and active carbons adsorption for the treatment of  
 565 simulated saline wastewater. Sep. Purif. Technol. 171, 101-111.  
 566 <https://doi.org/10.1016/j.seppur.2016.07.026>

567 Cho, M., Choi, Y., Park, H., Kim, K., Woo, G.J., Park, J., 2007. Titanium dioxide/UV disinfection  
 568 in fresh carrots, J. Food Prot. 70, 97-101. <https://doi.org/10.4315/0362-028x-70.1.97>  
 569

570 Coddington, J.W., Hurst, J.K., Lyman, S.V., 1999. Hydroxyl radical formation during peroxyxynitrous  
 571 acid decomposition. J. Am. Chem. Soc. 121, 2438-2443. <https://doi.org/10.1021/ja982887t>  
 572

573 Dariani, R.S., Esmaili, A., Mortezaali, A., Dehghanpour, S., 2016. Photocatalytic reaction and  
 574 degradation of methylene blue on TiO<sub>2</sub> nano-sized particles, Optik 127, 7143-7154.  
 575 <https://doi.org/10.1016/j.ijleo.2016.04.026>  
 576

577 Du, C.M., Sun, Y.W., Zhuang, X. F., 2008. The effects of gas composition on active species and  
 578 byproducts formation in gas–water gliding arc discharge. Plasma Chem. Plasma P. 28, 523–533.  
 579 <https://doi.org/10.1007/s11090-008-9143-1>

580 Gharib-Abou, S., Assadi, A.A., Costa, G., Bouzaza, A., Wolbert, D., 2016. Association of surface  
 581 dielectric barrier discharge and photocatalysis in continuous reactor at pilot scale: Butyraldehyde  
 582 oxidation, by-products identification and ozone valorization. Chem. Engin. J. 292, 276-283.  
 583 <https://doi.org/10.1016/j.cej.2016.02.029>

584 Ghodbane, H., Hamdaoui, O., Vandamme, J., Van Durme, J., Vanraes, P., Leys, C., Nikiforov, A.Y.,  
 585 2014. Degradation of AB25 dye in liquid medium by atmospheric pressure non-thermal plasma and  
 586 plasma combination with photocatalyst TiO<sub>2</sub>, Open Chem. 13, 325–331.  
 587 <https://doi.org/10.1515/chem-2015-0040>

588 Goldstein, S., Merényi, G., 2008. The Chemistry of Peroxynitrite: Implications for Biological  
 589 Activity. Methods Enzymol. 436, 49-61. [https://doi.org/10.1016/S0076-6879\(08\)36004-2](https://doi.org/10.1016/S0076-6879(08)36004-2)

590 Gurol, C., Ekinci, F.Y., Aslan, N., Korachi, M., 2012. Low temperature plasma for decontamination  
 591 of E. coli in milk. Int. J. Food Microbiol. 157, 1–5.  
 592 <https://doi.org/10.1016/j.ijfoodmicro.2012.02.016>

593 Hamrouni, A., Azzouzi, H., Rayes, A., Palmisano, L., Ceccato, R., Parrino, F., 2020. Enhanced solar  
 594 light photocatalytic activity of Ag doped TiO<sub>2</sub>-Ag<sub>3</sub>PO<sub>4</sub> composites. Nanomaterials. 10, 795.  
 595 <https://doi.org/10.3390/nano10040795>

596 He, D., Sun, Y., Xin, L., Feng, J., 2014. Aqueous tetracycline degradation by non-thermal plasma  
597 combined with nano-TiO<sub>2</sub>. Chem. Eng. J. 258, 18-25. <https://doi.org/10.1016/j.cej.2014.07.089>

598 Jiang, J., Tan, Z., Shan, C., Pan, J., Pan, G., Liu, Y., Chen, X., Wang, X., 2016. A new study on the  
599 penetration of reactive species in their mass transfer processes in water by increasing the electron  
600 energy in plasmas. Phys. Plasmas. 23, 103503. <https://doi.org/10.1063/1.4964364>

601

602 Khan, A.U., Kovacic, D., Kolbanovskiy, A., Desai, M., Frenkel, K., Geacintov, N.E., 2000. The  
603 decomposition of peroxyxynitrite to nitroxyl anion (NO<sup>-</sup>) and singlet oxygen in aqueous solution. PNAS.  
604 97, 2984–2989. <https://doi.org/10.1073/pnas.97.7.2984>

605

606 Kim, Y., Choi, Y., Kim, S., Park, J., Chung, M., Song, K.B., Hwang, I., Kwon, K., Park, J., 2009.  
607 Disinfection of iceberg lettuce by titanium dioxide–UV photocatalytic reaction. J. Food Prot. 72,  
608 1916–1922. <https://doi.org/10.4315/0362-028x-72.9.1916>

609

610 Kumar, J., Bansal, A., 2013. Photocatalysis by nanoparticles of titanium dioxide for drinking water  
611 purification: a conceptual and state-of-art review. Mater. Sci. Forum. 764, 130-150.  
612 <https://doi.org/10.4028/www.scientific.net/MSF.764.130>

613

614 Leduc, M., Guay, D., Coulombe, S., Leask, R.L., 2010. Effects of non-thermal plasmas on DNA and  
615 mammalian cells. Plasma Process. Polym. 7, 899–909. <https://doi.org/10.1002/ppap.201000032>

616

617 Liu, D.X., Liu, Z.C., Chen, C., Yang, A.J., Li, D., Rong, M.Z., Chen, H.L., Kong, M.G., 2016.  
618 Aqueous reactive species induced by a surface air discharge: Heterogeneous mass transfer and liquid  
619 chemistry pathways. Sci. Rep. 6, 23737. <https://doi.org/10.1038/srep23737>

620

621 Liu, F., Sun, P., Bai, N., Tian, Y., Zhou, H., Wei, S., Zhou, Y., Zhang, J., Zhou, W., Becker, K., Fang,  
622 J., 2010. Inactivation of bacteria in an aqueous environment by a direct-current, cold-atmospheric-  
623 pressure air plasma microjet. Plasma Process. Polym. 7, 231–236.  
624 <https://doi.org/10.1002/ppap.200900070>

625

626 Lubansky, A.S., Yeow, Y.L., Leong, Y.-K., Wickramasinghe, S.R., Han, B., 2006. A general method  
627 of computing the derivative of experimental data. AIChE J. 52, 323–332.  
628 <https://doi.org/10.1002/aic.10583>

629

630 Lukes, P., Clupek, M., Sunka, P., Peterka, F., Sano, T., Negishi, N., Matsuzawa, S., Takeuchi, K.,  
631 2005. Degradation of phenol by underwater pulsed corona discharge in combination with TiO<sub>2</sub>  
632 photocatalysis, Res. Chem. Intermed. 31, 285–294. <https://doi.org/10.1163/1568567053956734>

633

634 Lukes, P., Locke, B.R., Brisset, J.-L., 2012. Aqueous-phase chemistry of electrical discharge plasma  
635 in water and in gas–liquid environments, in: Parvulescu, V. I., Magureanu, M., Lukes, P. (Eds.),  
Plasma chemistry and catalysis in gases and liquids, Wiley-VCH, Weinheim, pp. 243–308.

636

637 Martinez, G.R., Di Mascio, P., Bonini, M.G., Augusto, O., Briviba, K., Sies, H., Maurer, P.,  
638 Roethlisberger, U., Herold, S., Koppenol, W.H., 2000. Peroxyxynitrite does not decompose to singlet  
639 oxygen (<sup>1</sup>ΔgO<sub>2</sub>) and nitroxyl (NO<sup>-</sup>). PNAS. 97, 10307–10312.  
<https://doi.org/10.1073/pnas.190256897>

640

641 Mei, D., Zhu, X., Chunfei, W., Ashford, B., Williams, P.T., Tu, X., 2016. Plasma-photocatalytic  
642 conversion of CO<sub>2</sub> at low temperatures: Understanding the synergistic effect of plasma-catalysis.  
App. Catal. B: Environ. 182, 552-553. <https://doi.org/10.1016/j.apcatb.2015.09.052>

643 Meireles, A., Giaouris, E., Simões, M., 2016. Alternative disinfection methods to chlorine for use in  
 644 the fresh-cut industry. *Food Res. Int.* 82, 71–85. <https://doi.org/10.1016/j.foodres.2016.01.021>  
 645

646 Misra, N.N., Schlüter, O., Cullen, P. J., 2016. Cold plasma in food and agriculture: Fundamentals  
 647 and applications, Academic Press, Amsterdam., <https://doi.org/10.1016/C2014-0-00009-3>  
 648

649 Mitoraj, D., Lamdab U., Kangwansupamonkon, W., Pacia, M., Macyk, W., Wetchakun, N.,  
 650 Beranek, R., 2018. Revisiting the problem of using methylene blue as a model pollutant in  
 651 photocatalysis: The case of InVO<sub>4</sub>/BiVO<sub>4</sub> composites. *J. Photochem. Photobiol. A: Chem.* 366,  
 652 103–110. <https://doi.org/10.1016/j.jphotochem.2018.02.023>  
 653

654 Moreau, M., Feuilleley, M.G.J., Veron, W., Meylheuc, T., Chevalier, S., Brisset, J.-L., Orange, N.,  
 655 2007. Gliding arc discharge in the potato pathogen *Erwinia carotovora* subsp. *atroseptica*: Mechanism  
 656 of lethal action and effect on membrane-associated molecules. *Appl. Environ. Microbiol.* 73, 5904–  
 657 5910. <https://doi.org/10.1128/AEM.00662-07>  
 658

659 Moreau, M., Orange, N., Feuilleley, M., 2008. Non-thermal plasma technologies: new tools for bio-  
 660 decontamination. *Biotechnol. Adv.* 26, 610–617. <https://doi.org/10.1016/j.biotechadv.2008.08.001>

661 Ochiai, T., Hayashi, Y., Ito, M., Nakata, K., Murakami, T., Morito, Y., Fujishima, A., 2012. An  
 662 effective method for a separation of smoking area by using novel photocatalysis-plasma synergistic  
 663 air-cleaner. *Chem. Engin. J.* 209, 313–317. <https://doi.org/10.1016/j.cej.2012.07.139>

664 Palau, J., Assadi, A.A., Peña-roja, J.M., Bouzaza, A., Wolbert, D., Martínez-Soria, V., 2015.  
 665 Isovaleraldehyde degradation using UV photocatalytic and dielectric barrier discharge reactors, and  
 666 their combinations. *J. Photochem. Photobiol. A: Chem.* 299, 110–117.  
 667 <https://doi.org/10.1016/j.jphotochem.2014.11.013>

668 Parrino, F., Camera-Roda, F., Loddo, V., Palmisano, L., 2016. Elemental bromine production by TiO<sub>2</sub>  
 669 photocatalysis and/or ozonation. *Angew. Chem. Int. Ed.* 55, 0391–10395.  
 670 <https://doi.org/10.1002/anie.201603635>  
 671

672 Parrino, F., Camera-Roda, G., Loddo, V., Augugliaro, V., Palmisano, L., 2013. Photocatalytic  
 673 ozonation: Maximization of the reaction rate and control of undesired by-products. *App. Catal. B:*  
 674 *Environ.* 178, 37–43. <http://dx.doi.org/10.1016/j.apcatb.2014.10.081>  
 675

676 Parrino, F., Conte, P., De Pasquale, C., Laudicina, V.A., Loddo, V., Palmisano, L., 2017. Influence of  
 677 adsorbed water on the activation energy of model photocatalytic reactions. *J. Phys. Chem. C* 121, 4,  
 678 2258–2267. <https://doi.org/10.1021/acs.jpcc.6b11945>  
 679

680 Parrino, F., Corsino, S.F., Bellardita, M., Loddo, V., Palmisano, L., Torregrossa, M., Viviani, G.,  
 681 2019b. Sequential biological and photocatalysis based treatments for shipboard slop purification: A  
 682 pilot plant investigation. *Process Saf. Environ. Prot.* 125, 288–296.  
 683 <https://doi.org/10.1016/j.psep.2019.03.025>  
 684

685 Parrino, F., De Pasquale, C., Palmisano, L., 2019. Influence of surface-related phenomena on  
 686 mechanism, selectivity, and conversion of TiO<sub>2</sub>-induced photocatalytic reactions, *ChemSusChem.*  
 687 12, 589–602. <https://doi.org/10.1002/cssc.201801898>  
 688

689 Parrino, F., Livraghi, S., Giamello, E., Palmisano, L., 2018. The existence of nitrate radicals in  
690 irradiated TiO<sub>2</sub> aqueous suspensions in the presence of nitrate ions. *Angew. Chem. Int. Ed.* 57,  
691 10702-10706. <https://doi.org/10.1002/anie.201804879>

692 Parrino, F., Loddo, V., Augugliaro, V., Camera-Roda, G., Palmisano, G., Palmisano, L., 2019.  
693 Heterogeneous photocatalysis: guidelines on experimental setup, catalyst characterization,  
694 interpretation, and assessment of reactivity, *Catal. Rev. Sci. Eng.* 61, 163-213.  
695 <https://doi.org/10.1080/01614940.2018.1546445>

696 Pavlovich, M.J., Chang, H.-W., Sakiyama, Y., Clark, D.S., Graves, D.B., 2013. Ozone correlates with  
697 antibacterial effects from indirect air dielectric barrier discharge treatment of water. *J. Phys. D: Appl.*  
698 *Phys.* 46, 145202. <https://doi.org/10.1088/0022-3727/46/14/145202>

699  
700 Perinban, S., Orsat, V., Raghavan, V., 2019. Nonthermal plasma–liquid interactions in food  
701 processing: A review. *Comp. Rev. Food Sci. F.* 18, 1985-2008. [https://doi.org/10.1111/1541-](https://doi.org/10.1111/1541-4337.12503)  
702 [4337.12503](https://doi.org/10.1111/1541-4337.12503)

703  
704 Ragni, L., Berardinelli, A., Iaccheri, E., Gozzi, G., Cevoli, C., Vannini, L., 2016. Influence of the  
705 electrode material on the decontamination efficacy of dielectric barrier discharge gas plasma  
706 treatments towards *Listeria monocytogenes* and *Escherichia coli*. *Innov. Food Sci. Emerg. Technol.*  
707 37, 170–176. <https://doi.org/10.1016/j.ifset.2016.07.029>

708  
709 Ragni, L., Berardinelli, A., Vannini, L., Montanari, C., Sirri, F., Guerzoni, M.E., Guarnieri, A., 2010.  
710 Non-thermal atmospheric gas plasma device for surface decontamination of shell eggs. *J. Food Eng.*  
711 100, 125–132. <https://doi.org/10.1016/j.jfoodeng.2010.03.036>

712  
713 Ryu, J., Choi, W., 2008. Substrate-specific photocatalytic activities of TiO<sub>2</sub> and multiactivity test for  
714 water treatment application. *Environ. Sci. Technol.* 42, 1, 294–300.  
715 <https://doi.org/10.1021/es071470x>

716  
717 Saha, A., Goldstein, S., Cabelli, D., Czapski, G., 1998. Determination of optimal conditions for  
718 synthesis of peroxyxynitrite by mixing acidified hydrogen peroxide with nitrite. *Free Radic. Biol.*  
*Med.* 24, 653-639. [https://doi.org/10.1016/s0891-5849\(97\)00365-1](https://doi.org/10.1016/s0891-5849(97)00365-1)

719  
720 Satuf, M.L., Brandi, R.J., Cassano, A.E., Alfano, O.M., 2005. Experimental method to evaluate the  
721 optical properties of aqueous titanium dioxide suspensions. *Ind. Eng. Chem. Res.* 44, 6643-6649.  
722 <https://doi.org/10.1021/ie050365y>

723  
724 Selma, M.V., Allende, A., López-Gálvez, F., Conesa, M.Á., Gil, M.I., 2008. Heterogeneous  
725 photocatalytic disinfection of wash waters from the fresh-cut vegetable industry, *J. Food Prot.* 71,  
726 286–292. <https://doi.org/10.4315/0362-028x-71.2.286>

727  
728 Shen, J., Tian, Y., Li, Y., Ma, R., Zhang, Q., Zhang, J., Fanf, J., 2016. Bactericidal effects against *S.*  
729 *aureus* and physicochemical properties of plasma activated water stored at different temperatures. *Sci.*  
*Rep.* 6, 28505. <https://doi.org/10.1038/srep28505>

730  
731 Sun, P., Wu, H., Bai, N., Zhou, H., Wang, R., Feng, H., Zhou, W., Zhang, J., Fang, J., 2012.  
732 Inactivation of *Bacillus subtilis* spores in water by a direct-current, cold atmospheric-pressure air  
plasma microjet. *Plasma Process. Polym.* 9, 157–164. <https://doi.org/10.1002/ppap.201100041>



733 Tang, S., Yuan, D., Rao, Y., Zhang, J., Qu, Y., Gu, J., 2018. Evaluation of antibiotic oxytetracycline  
734 removal in water using a gas phase dielectric barrier discharge plasma. *Journal Environ. Manage.*  
735 226, 22–29. <https://doi.org/10.1016/j.jenvman.2018.08.022>  
736

737 Tarabová, B., Lukeš, P., Hammer, M.U., Jablonowski, H., von Woedtke, T., Reuter, S., Machala, Z.,  
738 2019. Fluorescence measurements of peroxyxynitrite/ peroxyxynitrous acid in cold air plasma treated  
739 aqueous solutions. *Phys. Chem. Chem. Phys.* 21, 8883–8896. <https://doi.org/10.1039/C9CP00871C>  
740

741 Thøgersen, J., Kissner, R., Nauser, T., Koppenol, W.H., Richter, B., Jensen, F., Keiding, S.R., Knak  
742 Jensen, S.J., 2015. Primary photochemistry of peroxyxynitrite in aqueous solution. *Chem. Phys. Letters.*  
743 641, 187–192. <https://doi.org/10.1016/j.cplett.2015.10.056>  
744

745 Tian, W., Kushner, M.J., 2014. Atmospheric pressure dielectric barrier discharges interacting with  
746 liquid covered tissue. *J. Phys. D: Appl. Phys.* 47, 165201. [https://doi.org/10.1088/0022-](https://doi.org/10.1088/0022-3727/47/16/165201)  
747 3727/47/16/165201  
748

749 Tian, Y., Ma, R., Zhang, Q., Feng, H., Liang, Y., Zhang, J., Fang, J., 2015. Assessment of the  
750 physicochemical properties and biological effects of water activated by non-thermal plasma above  
751 and beneath the water surface, *Plasma Process. Polym.* 12, 439–  
752 449. <https://doi.org/10.1002/ppap.201400082>  
753

754 Toledano Garcia, D., Ozer, L.Y., Parrino, F., Ahmed, M., Brudecki, G.P., Hasan, S.W., Palmisano,  
755 G., 2018. Photocatalytic ozonation under visible light for the remediation of water effluents and its  
756 integration with an electro-membrane bioreactor. *Chemosphere* 209, 534–541.  
757 <http://dx.doi.org/10.1016/j.chemosphere.2018.05.197>

758 Vorontsov, A.V., Lyulyukin, M.N., Besov, A. S., 2012. Abatement of air pollutants in combined  
759 plasma and photocatalytic systems, *Global J. Environ. Sci. Technol.* 2, 3.

760 Wolfe, W.C., 1962. Spectrophotometric determination of hydrogen peroxide in diethyl ether. *Anal.*  
761 *Chem.* 34, 1328–1330. <https://doi.org/10.1021/ac60190a040>  
762

763 Yan, X., Ohno, T., Nishijima, K., Abe, R., Ohtani, B., 2006. Is Methylene Blue an appropriate  
764 substrate for a photocatalytic activity test? A study with visible-light responsive titania, *Chem. Phys.*  
765 *Lett.* 429, 606–610. <https://doi.org/10.1016/j.cplett.2006.08.081>  
766

767 Yeow, Y.L, Wickramasinghe, S.R., Han, B., Leong, Y.-K., 2003. A new method of processing the  
768 time-concentration data of reaction kinetics. *Chem. Eng. Sci.* 58, 3601–3610.  
769 [https://doi.org/10.1016/S0009-2509\(03\)00263-X](https://doi.org/10.1016/S0009-2509(03)00263-X)

770 Yousfi, M., Merbahi, N., Sarrette, J.P., Eichwald, O., Ricard, A., Gardou, J.P., Benhenni, M., 2011.  
771 Non thermal plasma sources of production of active species for biomedical uses: Analyses,  
772 optimization and prospect, in: Fazel-Rezai, R. (Eds.), *Biomedical engineering-frontiers and*  
773 *challenges*, InTech, Rijeka, pp. 99–124.

774 Yusupov, M., Neyts, E.C., Simon, P., Berdiyrov, G., Snoeckx, R., Van Duin, A.C.T., Bogaerts, A.,  
775 2013. Reactive molecular dynamics simulations of oxygen species in a liquid water layer of interest  
776 for plasma medicine. *J. Phys. D: Appl. Phys.* 47, 025205. [https://doi.org/10.1088/0022-](https://doi.org/10.1088/0022-3727/47/2/025205)  
777 3727/47/2/025205  
778

779 Zadi, T., Assadi, A., Nasrallah, N., Bouallouche, R., Nguyen-Tri, P., Bouzaza, A., Azizi, M., Maachi,  
780 R., Wolbert, D., Assadi, A., 2018. Treatment of hospital indoor air by a hybrid system of combined  
781 plasma with photocatalysis: Case of trichloromethane, an hybrid system of combined plasma with  
782 photocatalysis for treatment of hospital indoor air. *Chem. Eng. J.* 349, 276-286.  
783 <https://doi.org/10.1016/j.cej.2018.05.073>

784 Zhou, R., Zhou, R., Prasad, K., Fang, Z., Speight, R., Bazaka, K., Ostrikov, K.K., 2018. Cold  
785 atmospheric plasma activated water as a prospective disinfectant: The crucial role of peroxyne.  
786 *Green Chem.* 20, 5276–5284. <https://doi.org/10.1039/C8GC02800A>

787 Zhou, R., Zhou, R., Zhang, X., Li, J., Wang, X., Chen, Q., Yang, S., Chen, Z., Bazaka, K., Ostrikov,  
788 K., 2016. Synergistic Effect of Atmospheric-pressure Plasma and TiO<sub>2</sub> Photocatalysis on Inactivation  
789 of *Escherichia coli* Cells in Aqueous Media, *Sci. Rep.* 6, 39552. <https://doi.org/10.1038/srep39552>

790 Zhou, R., Zhou, R., Zhang, X., Zhuang, J., Yang, S., Bazaka, K., Ostrikov, K., 2016b. Effects of  
791 atmospheric-pressure N<sub>2</sub>, He, air, and O<sub>2</sub> microplasmas on Mung Bean seed germination and seedling  
792 growth. *Sci. Rep.* 6, 32603. <https://doi.org/10.1038/srep32603>

793 Zhu, Z., Cai, H., Sun, D.-W., 2018. Titanium dioxide (TiO<sub>2</sub>) photocatalysis technology for  
794 nonthermal inactivation of microorganisms in foods. *Trends Food Sci. Tech.* 75, 23-35.  
795 <https://doi.org/10.1016/j.tifs.2018.02.018>  
796